Activation cross section for the $(n, 2n)$ and (n, p) reactions on ^{103}Rh, ^{48}Ti and ^{52}Cr from reaction threshold up to 25 MeV energy region

R.K. Singh [a,*], N.L. Singh [a,b,**], Mayur Mehta [a,c], Rakesh Chauhan [a], S.V. Suryanarayana [d], Rajnikant Makwana [a], B.K. Nayak [d], H. Naik [e], Jan Varmuza [f], K. Katovsky [f]

[a] Department of Physics, Faculty of Science, The M. S. University of Baroda, Vadodara, 390002, India
[b] Department of Physics, Netaji Subhas University of Technology, Dwarka, Delhi, 110078, India
[c] Institute for Plasma Research, Gandhinagar, 382428, India
[d] Nuclear Physics Division, Bhabha Atomic Research Centre, Mumbai, India
[e] Radiochemistry Division, Bhabha Atomic Research Centre, Mumbai, India
[f] Department of Electrical Power Engineering, Brno University of Technology, Brno, 61600, Czech Republic

ARTICLE INFO

ABSTRACT

Activation and off-line γ-ray spectrometric methods were used to measure the ground and isomeric state $(n, 2n)$ reaction cross section for ^{103}Rh at two different neutron energies. The standard ^{27}Al $(n, \alpha)^{24}$Na reference reaction was used to normalise neutron flux. The proton beam from the 14UD BARC-TIFR Pelletron facility in Mumbai, India, was utilised to create high-energy quasi-monoenergetic neutrons via the ^{7}Li (p, n) reaction. Statistical model calculations including the level density, pre-equilibrium and optical potential model were performed using the TALYS (ver. 1.95) and EMPIRE (ver. 3.2.3) reaction codes. In addition, because of considerable discrepancies in measured data, the literature (n, p) reaction cross section of ^{52}Cr and ^{48}Ti targets were examined theoretically in the present work. The measured cross sections are discussed and compared with the latest evaluated data of the FENDL-3.2b, CENDL-3.2, TENDL-2019, JENDL-5.0, and ENDF/B-VIII.0 libraries, and experimental data based on the EXFOR compilation. The theoretical investigation of the $(n, 2n)$ reaction cross section was performed for the ground and isomeric state for the first time from reaction threshold to 25 MeV energies. The experimental data corresponding to the ground, isomeric state and isomeric ratio were reproduced consistently by the theoretical calculations. The present experimental results are good with certain literature data and theoretical values.

1. Introduction

Studies of neutron induced reactions are of immense interest in reactor applications. In a reactor, when neutrons originated from fusion or fission reactions interact with its structural materials, control rods, fuel and shielding materials, and change the mechanical and physical properties of these materials. Therefore, it is necessary to have cross section data for these materials at all possible neutron energies. This nuclear data is required for calculating nuclear heating, induced radio-activity, nuclear transmutation rates, and radiation damage caused by gas production on prospective first wall material. The fusion reaction of deuterium and tritium (D-T) produces α particles and neutrons. The high-energy (14 MeV) neutrons produced from the fusion reaction,

transfer their energy to the breeding blanket and the reactor's first wall. The measured experimental data of fusion reactor structural materials and evaluated data from different libraries show a large discrepancy in cross section data at the same incident neutron energy. Therefore, accurate activation cross section data at 14–15 MeV neutron energies are needed to design, construct, and evaluate the fusion reactor. The structural materials studies are now also considered for accelerator-driven subcritical systems (ADSs) and the fourth-generation nuclear reactor (Swedish Nuclear Fuel and Waste, 2008).

The systematic study of gas-producing reaction (n, p) is needed because this reaction is harmful to the mechanical stability of the reactor. The existing data for this reaction was inconsistent and could not be used to resolve the discrepancy. The (n, p) reactions on Cr and Ti

---

* Corresponding author.
** Corresponding author. Department of Physics, Faculty of Science, The M. S. University of Baroda, Vadodara, India.
  E-mail addresses: ratankumar339@gmail.com (R.K. Singh), nl.singh-phy@msubaroda.ac.in (N.L. Singh).
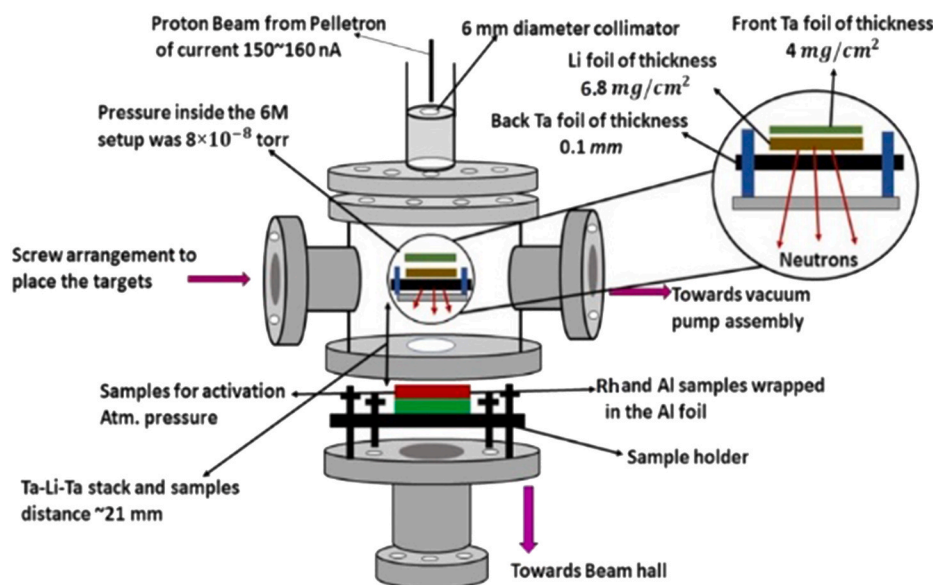
Fig. 1. A systematic arrangement of the experimental setup is used for the irradiation of the samples.

isotopes have been studied for many years. Titanium alloys are desirable structural materials for fusion reactors because of their great characteristics. Titanium has a high strength-to-weight ratio, intermediate strength values, good fatigue and creep rupture properties, small modulus of elasticity, high electrical resistivity, heat capacity, low coefficient of thermal expansion, low long-term residual radioactivity, high corrosion resistance, good compatibility with coolants such as lithium, helium, and water, high workability and weldability, and commercial availability with established mine and mill facilities. Since chromium is an important constituent of structural steel, its activation data is important for practical applications in fusion reactor technology ~e.g., estimation of activity level, hydrogen and helium gas production, nuclear heating, and radiation damage. Compound nucleus (CN), Direct and Pre-equilibrium reaction channels play an important role at neutron energies up to 20 MeV. Therefore, measured cross sections with better accuracy are needed for the understanding of these reaction channels. Recently, several articles on nuclear reactions at moderate excitation energies have been concerned with the emission of particles before the nucleus reaches statistical equilibrium. In theoretical calculations from statistical codes, selecting suitable models is important for obtaining the correct cross sections values (Singh et al., 2021; Hecker et al., 1989).

This paper reports experimental $(n, 2n)$ excitation functions for rhodium nuclei for the neutron energies up to 25 MeV. To understand the reaction mechanism, the data have been compared to a model, which permits pre-equilibrium and statistical modes of decay. This cross section of data is useful for developing the theoretical model and explaining the reaction mechanism. Rhodium is an inert transition metal, which has single naturally occurring isotopes ^{103}Rh (100%) and is used as an alloying agent to harden palladium and platinum. The ^{103}Rh is used for radiochemical diagnosis of integrated neutron fluence since nuclear reactions (n, γ), $(n, 2n)$ and $(n, 3n)$ lead to different radioactive isotopes of rhodium with lifetimes in the useful range for activation measurements. Threshold reactions including (n, n') and $(n, 2n)$ have been used extensively for determining the differential flux (dQ/dE) from neutron sources by foil activation techniques. The cross sections of (n, xn) reactions are necessary for activation detectors which are used to probe energy components of neutron fluence. An example of such a detector is rhodium, which is monoisotopic (Georgali et al., 2018).

In the present work, the $(n, 2n)$ cross section for the ^{103}Rh target was measured at two different neutron energies relative to the standard ^{27}Al $(n, \alpha)^{24}$Na reference reaction. The experimental results from the present work were compared with the literature data available in the EXFOR

database (Otuka Dupont et al., 2014) and evaluated data of the ENDF/B-VIII.0, JENDL-5.0, FENDL-3.2b, CENDL-3.2 and TENDL-2019 libraries (Brown Chadwick et al., 2018; Ge et al., 2020; Koning Rochman et al., 2019; Iwamoto Shibata et al., 2022; Forrest et al., 2022). The nuclear reaction codes TALYS (ver. 1.95) and EMPIRE (ver. 3.2.3) were used for the theoretical estimation of the reaction cross section using different level density and pre-equilibrium models. Furthermore, the systematic theoretical study of cross sections for fusion reactor structure materials ^{48}Ti and ^{52}Cr was performed by the TALYS code. We optimize the level density parameters of the phenomenological and microscopic models in the TALYS code to obtain the best possible descriptions of the ^{48}Ti and ^{52}Cr experimental data. The statistical model calculations were discussed and compared with the available experimental and evaluated data.

2. Experimental procedure

2.1. Sample preparation and irradiations details

The irradiations of the targets were carried out using experimental facilities at the 14UD BARC-TIFR Pelletron Linac accelerator facility in Mumbai, India. The ^{7}Li (p, n) reaction was used to produce the quasi-monoenergetic neutrons of energy 16.86 and 19.89 MeV. The proton beam energies of 19 and 22 MeV and current of 150–160 nA were incident on a 6.8 mg/cm^2 lithium (Li) foil, which is sandwiched between the two Tantalum (Ta) foil. The front tantalum foil, which is facing the proton beam was the thinnest and have a thickness of 4 mg/cm^2 and the back tantalum foil of thickness 0.1 mm was used to stop the proton beam. The experimental setup for irradiation of the samples is shown in Fig. 1. The sandwich ^{7}Li targets were kept in a vacuum at an angle of 0° relative to the primary proton beam and 2.1 cm from the target center. The pressure of the vacuum was kept constant at 8×10^{-8} torr via a micrometric valve, whereas in the neutron activation zone, it was atmospheric. For irradiation, high-purity natural rhodium metallic samples (~99.9%), areas of 0.9 to 0.8 cm^2, thickness of 0.23 mm and weighing 0.256 g each were taken. The sample used for neutron irradiation was wrapped in the 0.025 mm thick aluminium foil used to prevent radioactive contamination from each other. Each rhodium sample was sandwiched between two aluminium foils. The reference sample was the thin metallic foil of aluminium (~99.9%), area of 1 cm^2 and 0.11 mm in thickness, each containing 0.03 g of aluminium. The sandwiched samples were irradiated one at a time with the neutron

Table 1

The spectroscopic decay data of measured reaction products of ^{102}Rh and ^{24}Na nuclei.

Nuclear reactions	E_{th} (MeV)	Half-life ($\tau_{1/2}$)	Decay Mode	E_γ (keV)	I_γ (%)
^{103}Rh $(n, 2n)^{102}$Rh^m	9.55	3.742 y (10)	ε (99.77%)	697.5	44.0 (20)
			IT (0.23%)	766.8	34.0 (20)
				1112.8	19.0 (10)
^{103}Rh $(n, 2n)^{102}$Rh^g	9.41	207.3 day (17)	ε (78%) β^- (22%)	468.6	2.90 (20)
^{27}Al $(n,\alpha)^{24}$Na	3.25	14.997 h (12)	β^- (100%)	1368.62	99.94 (4)
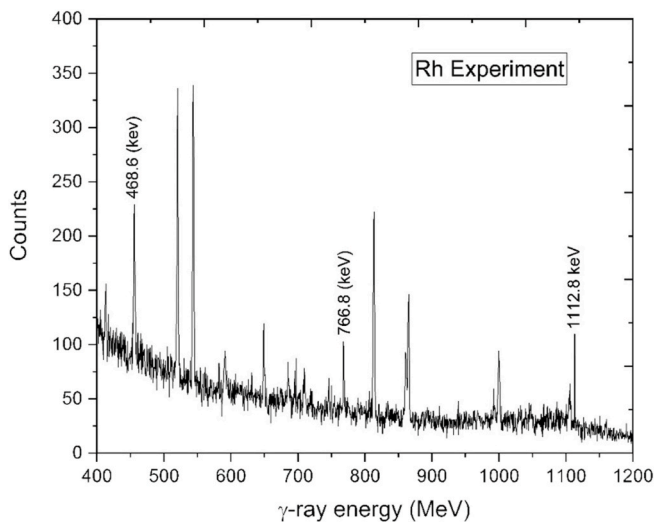
Fig. 2. The off-line γ-ray spectra of the irradiated Rh sample at 22 proton energies.

Table 2

Measured values of fitting parameters of the HPGe detector efficiencies.

Fitting parameters	parameter values	E_γ (keV)	Efficiencies
ε_0	0.06751 ± 0.00373	468.6	0.01926
ε_c	0.00377 ± 0.0007243	697.5	0.01153
E_0	335.39 ± 32.384	766.8	0.01014
		1112.8	0.0065
		1368.63	0.00554

beam for a period of 5–6 h to obtain sufficient activity in the samples.

2.2. Measurement of radioactivity

After each irradiation, the induced activity of the rhodium targets and reference foils were measured using an HPGe coaxial detector. To enhance the counting rate, the close measuring geometry was adopted in the experiment. The neutron irradiated activated samples emit γ-rays and these γ-rays were counted with a pre-calibrated 80 cm^3 and 16% relative efficiency HPGe detector coupled to a PC based 4096 multi-channel analyzer. The γ-ray spectra measured were analysed by the Genie gamma analysis software. Table 1 shows the decay data of the product nuclei of the rhodium target and reference monitor foil aluminium, as taken out from the NuDat 2.8 database (Firestone, 2007; De Frenne, 2009).

The standard point source ^{152}Eu was used for the efficiency calibration of the γ-ray detector. The energy resolution full width at half
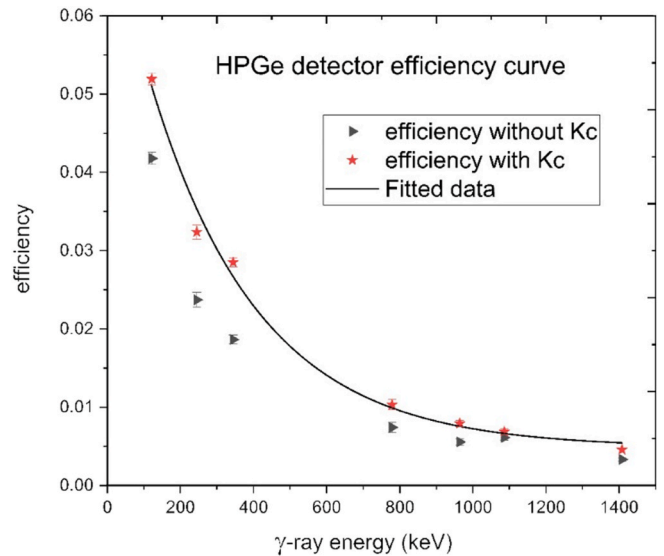
Fig. 3. Absolute efficiency curve of the HPGe detector with and without correction factor (Kc) for the ^{152}Eu point source.

maximum at 1408.6 keV of ^{152}Eu point like solid source was 1.9 keV for the HPGe detector. The samples were placed at a suitable distance from the end cap of the detector, to ensure a dead time of less than 5% and to minimize the coincidence summing effect. The γ-ray spectra of the rhodium sample at the 22 MeV energy proton irradiation are shown in Fig. 2. The efficiencies were obtained using the standard equation $\varepsilon(\gamma) = CK_c / (N_0 I_\gamma e^{-\lambda t})$ where $\varepsilon(\gamma)$ is the efficiency of the corresponding γ-rays, C is the count under gamma peak, N_0 activity of standard ^{152}Eu source at an initial time, I_γ is the γ-ray intensity, λ is the decay constant of ^{152}Eu, and K_C is the correction factor for the coincidence summing effect, t is the time elapsed from the manufacturer date to the start of counting. The efficiencies of the HPGe detector were interpolated through the following fitting function (1) and shows a good fit with a R^2 value of 0.9954 and $\chi^2 = 5.959$.

$$\varepsilon(E) = \varepsilon_0 * exp(-E / E_0) + \varepsilon_c \tag{1}$$

where, ε_0, E_0 and ε_c are the fitting parameter and values along with calculated efficiencies for characteristics γ-lines of 475.06 and 1368.62 keV, which are given in Table 2. The fitted efficiency curve of the HPGe detector with and without correction factor (Kc) is shown in Fig. 3.

2.3. Mean neutron energies and flux

The reaction ^{7}Li (p, n) was used to produce fast quasi-monoenergetic neutrons. This reaction ^{7}Li $(p, n)^7$Be produces monoenergetic neutrons below 2.4 MeV proton energies. However, above the proton energy of 2.4 MeV, the first excited state of ^{7}Be at 0.43 MeV excited, which produces the second group of neutrons (n_1). In ^{7}Li (p, n) reaction, for the proton energy below 5 MeV the zero-degree yield of these low energy neutrons is less than about 10% of the ground state yield. Thus, the usefulness of the monoenergetic neutron source is only slightly impaired. The three-body breakup reaction ^{7}Li $(p, n3He)^4$He takes place at above 3.68 MeV, which contributes neutrons with primary neutron peak (n_0). The threshold for the reaction ^{7}Li $(p, n)^7$Be is 7.06 MeV, above 7.06 MeV the second excited of ^{7}Be also contributes to the primary neutron group. The primary neutron peak (n_0) has higher neutron energy and flux, and this peak is used to measure the $(n, 2n)$ reactions cross section. The neutron spectra at 15, 20 and 30 MeV proton energies for the ^{7}Li target and at 39.3 MeV proton energies for ^{6}Li and ^{7}Li targets are given in Ref. (McNaughton King et al., 1975; Jungerman Brady et al., 1971). Similarly, Uwamino Soewarsono et al. (1997) gives neutron
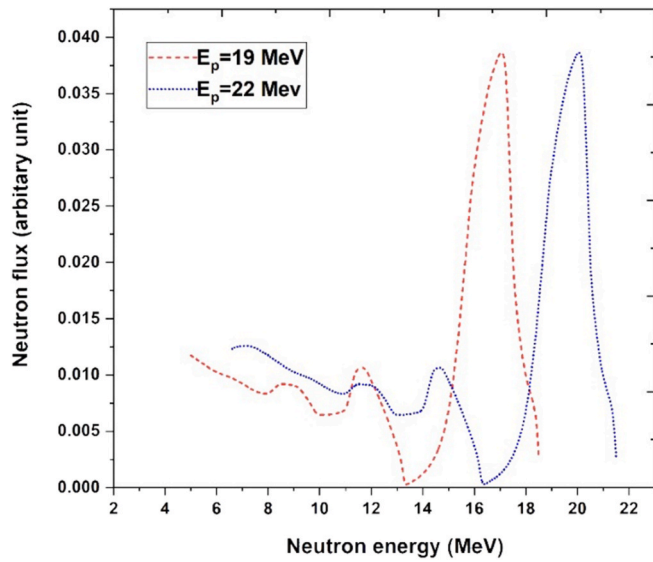
Fig. 4. Neutron spectra at 19 and 22 MeV proton energies obtained by McNaughton et al. (McNaughton King et al., 1975).

Table 3
Measured correction factors for the sample and monitor reaction.

$\langle E_n \rangle \pm \Delta E_n$ (MeV)	Γ_{attn}		C_{low}		C_g	
	Rh	Al	Rh	Al	Rh	Al
16.86 ± 0.55	0.98275	0.99922	0.9251	0.8645	1.0094	1.0038
19.89 ± 0.59	0.98182	0.99915	0.9016	0.6973	1.0099	1.0039

Table 4
Measured cross sections along with the isomeric cross section ratio with uncertainties.

$\langle E_n \rangle \pm \Delta E_n$ (MeV)	^{103}Rh $(n, 2n)^{102}$Rh^m (mb)	^{103}Rh $(n, 2n)^{102}$Rh^g (mb)	^{103}Rh $(n, 2n)^{102}$Rh (mb)	Ratio (σ_m/σ_g)
16.86 ± 0.55	745.68 ± 80.64	736.07 ± 50.93	1481.75 ± 131.57	1.013
19.89 ± 0.59	588.74 ± 63.04	446.73 ± 41.21	1035.47 ± 104.25	1.318

spectra at 20, 25, 30, 35 and 40 MeV proton energies for the ^{7}Li target and Brady and Romero, (1990) also provides zero degree cross section with proton energies for ^{6,7}Li (p, n) reaction. The different peaks and continuum contributions are separately analysed in the recent article by Midhun Musthafa et al. (2021) and we have also taken help of this to get the spectra at present measured energies as different contributions have energy dependences. The contribution for ^{6}Li is obtained using spectral shape, cross section and neutron yield given in Brady and Romero (1990). The contributions of ^{6,7}Li are added as per natural abundance and final spectra were obtained. The threshold for the ^{7}Li (p, n) reaction is 1.8 MeV and it is 5.9 MeV for the ^{6}Li (p,n) reaction, therefore the small contribution of ^{6}Li is seen around 4 MeV below the peak value. It is observed that 19 and 22 MeV spectra have negligible contributions and small visible differences at these proton energies, this obtained spectrum is given in Fig. 4. Therefore we have used only combined spectra in the manuscript. The neutron spectrum was used for the neutron energy calculation based on the kinematic relation ($E_n = E_p - E_{th}$) where, E_p is the proton energy and E_{th} threshold energy of the ^{7}Li (p, n) reaction. The effective average neutron energy of the primary neutron group from the neutron spectrum was calculated as mentioned in Smith et al. (2020) and the uncertainty associated with this neutron energy was calculated
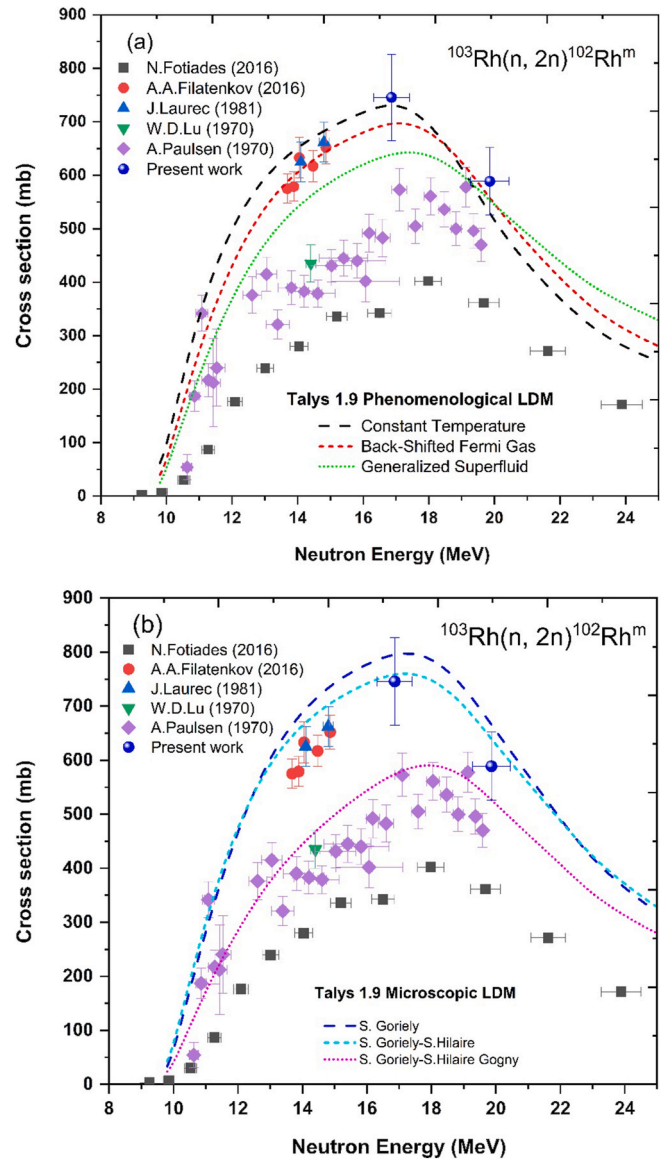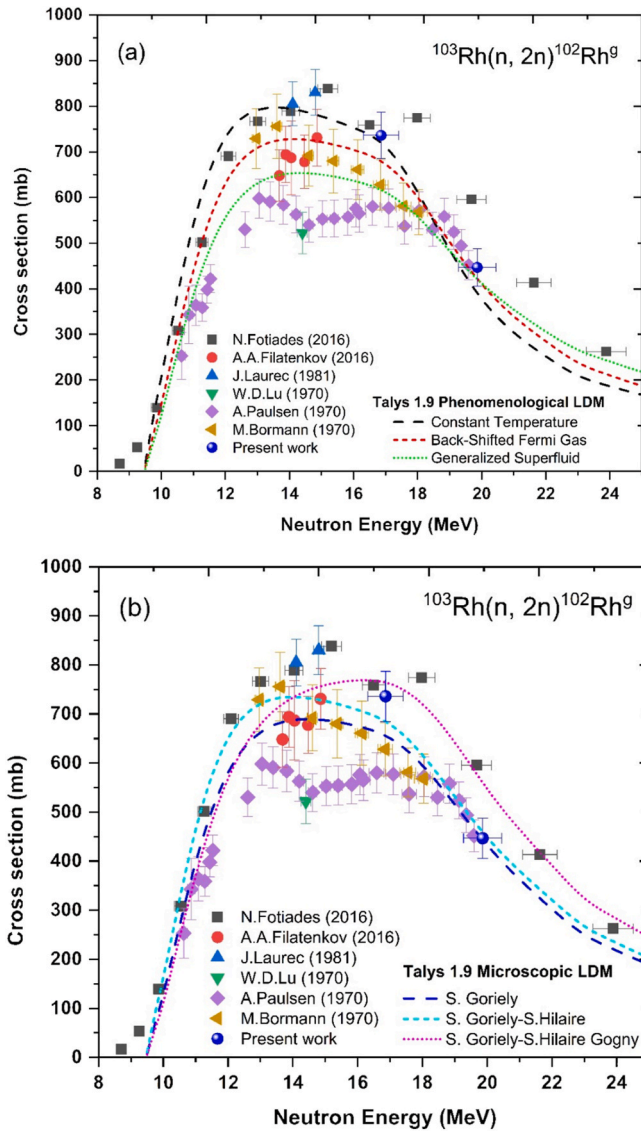

Fig. 5. Present measurements and reported literature isomeric state cross sections are compared with the TALYS (ver. 1.95) calculations based on the level density models.

from the width of the monoenergetic part of the spectra. The neutron flux was determined using the ^{27}Al $(n, \alpha)^{24}$Na reference reaction.

3. Data analysis

3.1. Measurements of the ^{103}Rh $(n, 2n)^{102}$Rh^{m,g} reaction cross section

The cross section of the ^{103}Rh $(n,2n)^{102}$Rh^{m,g} reaction was measured via the neutron activation technique.

$$\langle \sigma_r \rangle = \langle \sigma_m \rangle \left(\frac{C_r \lambda_r Wt_m AM_r Abu_m \varepsilon_m I_m f_m}{C_m \lambda_m Wt_r AM_m Abu_r \varepsilon_r I_r f_r} \right) \times \frac{(C_{attn} * C_{low} * C_g)_r}{(C_{attn} * C_{low} * C_g)_m} \quad (2)$$

where $\langle \sigma_r \rangle$ and $\langle \sigma_m \rangle$ is the reaction and monitor reaction cross sections, C_r and C_m is the detected photo-peak counts of the γ-ray of the reaction and monitor products, λ_r and λ_m is the decay constant of the reaction and monitor products nuclei, ε_r and ε_m is the efficiency for characteristic γ-ray of radionuclide of the reaction and monitor nuclei, I_r and I_m is the γ-ray abundance of the reaction and monitor, Wt_r and Wt_m is the weight of the reaction and monitor, Abu_r and Abu_m is the isotopic abundance of

Fig. 7. The present measurements and reported literature cross sections are compared with the latest evaluated data libraries.

correction factor for the break-up neutrons (C_{low}) was calculated from the spectral indexing method of Smith et al. (2020) and correction values for these three parameters are given in Table 3.

3.2. Uncertainty in the measured $^{103}Rh\ (n, 2n)^{102}Rh^{m,g}$ reaction cross section

The uncertainty in the measured cross section at two different energies was calculated by taking the square root of the quadratic sum of all the individual uncertainties involved in all parameters. Similarly, the uncertainty in the HPGe detector efficiency (ε_γ) has been propagated using the uncertainties of the counts (C), the activity (A), and the γ-ray abundance (I_γ) using the standard quadrature sum relation of error propagation. The error propagation expression for the measured cross section is written in Otuka et al. (2017). The uncertainties in the isotopic abundance, atomic mass, half-life and γ-ray abundances were taken from the National Nuclear data Center (NNDC) database. The uncertainties of different parameters contribute to the total uncertainty of the measured cross section. The source of uncertainty in the measured cross section and their values are listed below: Decay data (<0.35) %, counts of γ-peak (<9) %, the efficiency of γ-detector (<2.5) %, corrections for self-absorption and γ-cascade summing (<0.5) %, reference cross sections used for neutron fluence determination (<1%), sample mass (<0.1) %, isotopic abundance (<1.0%). The contribution of uncertainties of other parameters is very small and can be neglected. As can be seen, the uncertainty of the $^{103}Rh\ (n, 2n)^{102}Rh^m$ and $^{103}Rh\ (n, 2n)^{102}Rh^g$ reactions cross sections are in the range of 7–11%.

4. Statistical calculations

4.1. TALYS (ver. 1.95) code

The reaction cross section as a function of neutron energy was estimated using the computer code TALYS (ver. 1.95) (Koning et al., 2018). Many theoretical models, such as compound, pre-compound, and direct processes, have been developed to better explain nuclear reaction mechanisms. TALYS is a statistical nuclear reaction computer program that may be used to analyse and predict different nuclear reaction cross sections. Nuclear data generated by the code can be used in nuclear power reactors (GEN-IV), radioactive waste transmutation, fusion reactors, accelerator applications, medical isotope synthesis, radiation, and astronomy. The reaction cross sections were computed using

Fig. 6. Present measurements and reported literature ground state cross sections are compared with the TALYS (ver. 1.95) calculations based on the level density models.

the reaction and monitor, AM_r and AM_m is the atomic mass of the reaction and monitor, f_r and f_m is the time factor of the reaction and monitor products, C_{lowr} and C_{lowm} is the low energy background neutron correction factor of the reaction and monitor, C_{attnr} and C_{attnm} is the γ-ray self-attenuation correction factor of the reaction and monitor, C_{g_r} and C_{g_m} is the geometry correction factor of the reaction and monitor. The timing factor as specified in equation (2) is given as:

$$f = (1 - exp\ (-\lambda t_i))\ exp\ (-\lambda t_c)(1 - exp\ (-\lambda t_m))$$

where, t_i is irradiation time, t_c is cooling time and t_m is counting time.

The cross sections for the reference reaction $^{27}Al\ (n, \alpha)^{24}Na$ was calculated using the International Reactor Dosimetry and Fusion File (IRDFF-1.05) (Capote Zolotarev et al., 2014) data and by using a linear interpolation method at the nearest point energies. The corresponding cross sections at the neutron beam energies were obtained from the IRDFF-1.05 library and values are 80.98 ± 0.162 and 41.73 ± 0.194 (mb).

The correction factor for γ–ray self-attenuation factor (Γ_{attn}) for activated materials and the correction of the geometry (C_g) was calculated using the formula as mentioned in Singh et al. (2022), whereas the
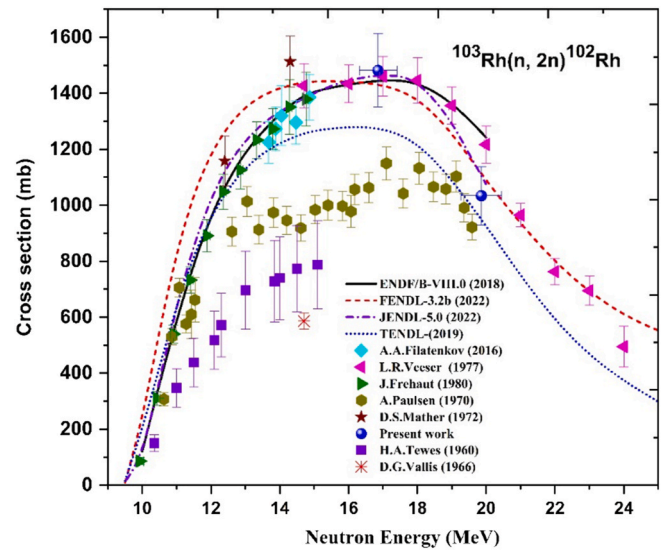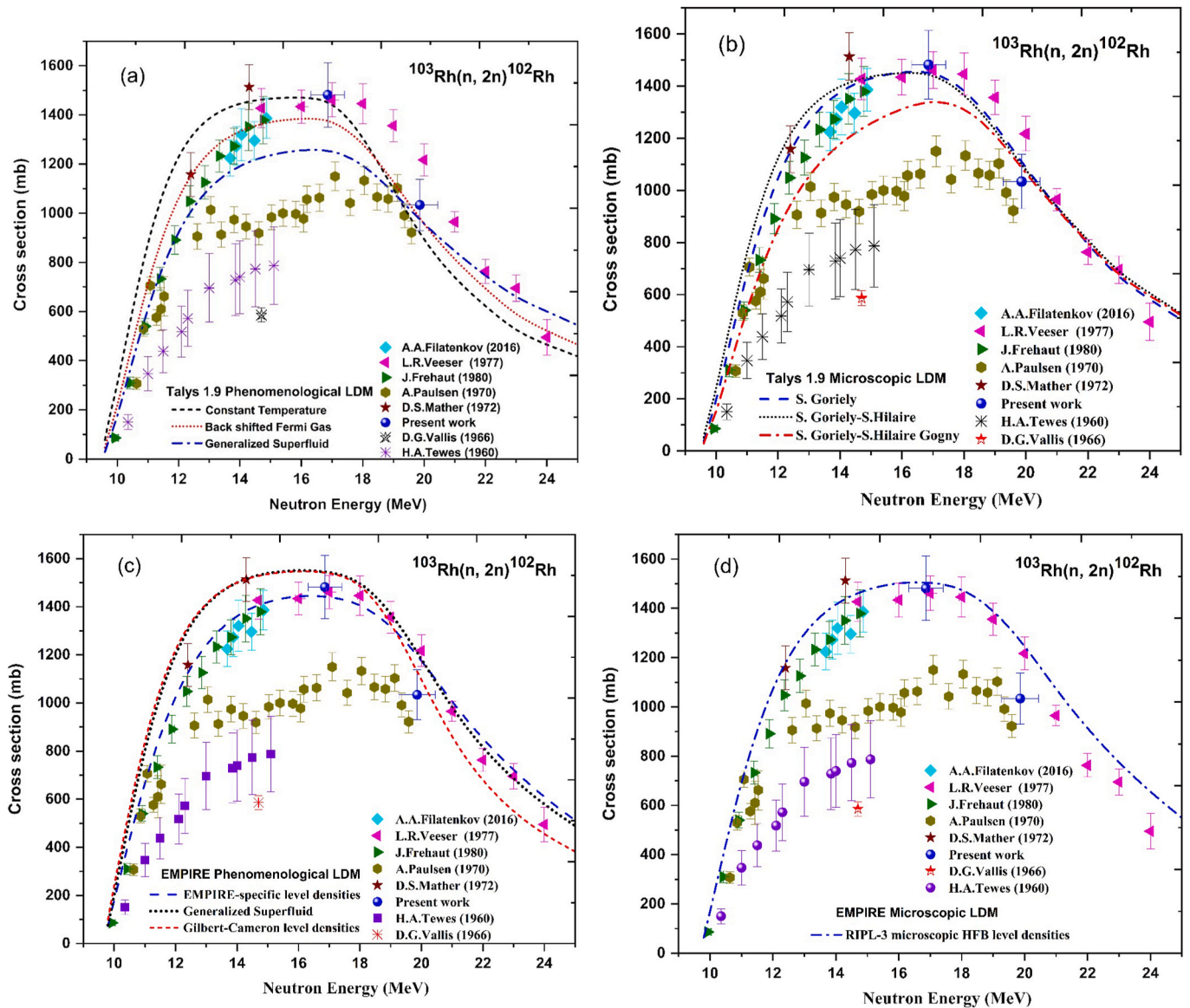
Fig. 8. Present measurements and reported literature cross sections are compared with the TALYS (ver. 1.95) and EMPIRE (ver. 3.2.3) calculations based on the level density models.

various input values in this code. The compound nucleus cross section was calculated using the statistical Hauser-Feshbach theory (Hauser and Feshbach, 1952). The optical model potential was parameterized using the Koning-Delaroche local potential, Koning-Delaroche global potential (Talys keyword 'localomp'), Koning-Delaroche local dispersive potential (Talys keyword 'dispersion y') (Koning and Delaroche, 2003), and Bauge-Delaroche JLM potential (Talys keyword 'jlmomp y') (Bauge et al., 2001). The exciton model was used to account for the role of pre-equilibrium emissions (Talys keyword 'preeqmode') (Kalbach, 1986; Koning and Duijvestijn, 2004). The Brink-Axel model was used to calculate the γ-ray strength functions for all transition types except for the E1 transition. For the E1 transition, Kopecky and Uhl's generalized Lorentzian form was employed (Brink, 1957; Axel, 1962; Kopecky and Uhl, 1990).

Three phenomenological level densities, the level density Constant Temperature Model (CTM) proposed by Gilbert and Cameron the excitation energy is split into two parts in this model: a lower energy component that follows the constant temperature rule and a higher energy part that follows the Fermi gas model (Gilbert and Cameron, 1965). The Fermi gas expression is employed in all energy regions in the

Back-shifted Fermi Gas Model (BFGM) (Dilg et al., 1973). The Generalized Superfluid Model (GSM) considers superconductive pairing correlations according to the Barden-Cooper-Schrieffer theory, *i.e.,* pairing correlations at low energy greatly impact the level density, and high energy area described by the Fermi gas model (Ignatyuk et al., 1979, 1993). There are three microscopic level densities. In ldmodel 4, for the RIPL-3 database, S. Goriely used Hartree-Fock computations to compute level densities from drip line to drip line for excitation energy up to 150 MeV and spin values up to I = 30 (Goriely et al., 2001). Nuclear structural features calculated inside the distorted Skyrme-Hartree-Fock-Bogolyubov framework are used in the computations of ldmodel 5. For excitation energy up to 200 MeV and spin values up to J = 49, level densities for over 8500 nuclei are given in the tabular format (Goriely et al., 2008a). The Gogny force is used in the ldmodel 6, which is based on temperature-dependent Hartree-Fock-Bogolyubov computations (Hilaire et al., 2012). It is observed that different phenomenological level density parameters are given in Talys code and these parameters were used in the calculations along with theoretical models. Similarly, two microscopic level density parameters 'ctable' and 'ptable' are mentioned in the Talys code with the default zero and these

Table 5

The statistical model codes used for theoretical calculations of the $(n, 2n)$ and (n, p) reactions cross section.

Statistical codes	Optical potential model	Level density models	Pre-equilibrium model	γ-ray strength function
EMPIRE (ver. 3.2.3)	Koning-Delaroche	Generalized superfluid Gilbert-Cameron Hartree-Fock-BCS	Exciton model (PCROSS)	Modified Lorentzian (MLO1)
TALYS (ver. 1.95)	Koning-Delaroche	Constant temperature Back-shifted Fermi gas Generalized superfluid S. Goriely S. Goriely-S. Hilaire S. Goriely-S. Hilaire Gogny force	preeqmode 2	Kopecky-Uhl

two were used in the theoretical calculations. A Talys keyword 'fullhf' was used for Hauser-Feshbach calculation using the full *j,l* coupling and 'gshell' keyword including the damping of shell effects with excitation energy in single-particle level densities.

4.2. EMPIRE (ver. 3.2.3) code

The theoretical estimations were also done with the EMPIRE (ver. 3.2.3) code (Herman et al., 2007). The compound nucleus (CN) reaction cross section was computed using the Hauser-Feshbach theory in the EMPIRE code. The direct reaction was calculated with the help of the ECIS06 program. The Hofmann, Richert, Tepel, and Weidenmuller model (HRTW) (Hofmann et al., 1975) was used to calculate the width fluctuation corrections up to the neutron energy of 3 MeV. The outgoing protons' optical potential model parameters were also retrieved from the RIPL-3 database (Capote Herman et al., 2009) using Koning and Delaroche (2003). The modified Lorentzian model available in the RIPL-3 database was used to describe the γ-ray strength function (Plujko, 2000). The cross sections were calculated using several level densities models, including (i) Generalized superfluid (ii) Gilbert-Cameron and (iii) Hartree-Fock-BCS (HF-BCS) method (Arrigo et al., 1994; Goriely et al., 2008). To account for pre-equilibrium emission at higher energies, the quantum-mechanical pre-equilibrium models (i) Multi-Step-Compound (MSC) (ii) Multi-Step-Direct model (MSD) and the phenomenological pre-equilibrium models (iii) Exciton model with default mean free path multiplier (MFP) (PCROSS = 1.5) (iv) Monte Carlo Hybrid (DDHMS) were included in theoretical calculations (Tamura et al., 1982; Nishioka et al., 1986).

5. Results and discussion

The ^{103}Rh $(n, 2n)^{102}$Rh^m, ^{103}Rh $(n, 2n)^{102}$Rh^g and ^{103}Rh $(n, 2n)^{102}$Rh reaction cross section was measured at two different neutron energies. The experimental results of the ^{103}Rh $(n, 2n)^{102}$Rh^m, ^{103}Rh $(n, 2n)^{102}$Rh^g reactions and for the total ^{103}Rh $(n, 2n)^{102}$Rh reaction which is the sum of the both are presented in Table 4. The cross sections were compared and discussed with previous literature data taken from the EXFOR compilation and evaluation of the FENDL-3.2b, TENDL-2019, JENDL-5.0 and ENDF/B-VIII.0 libraries. Statistical reaction codes TALYS (ver. 1.95) and EMPIRE (ver. 3.2.3) were used for the theoretical estimations of the reaction cross sections. It is observed that most of the previous measurements were made with β-ray or γ-ray counting using NaI(T1) detector. The γ-ray counting with NaI(T1) detector suffers from a defect
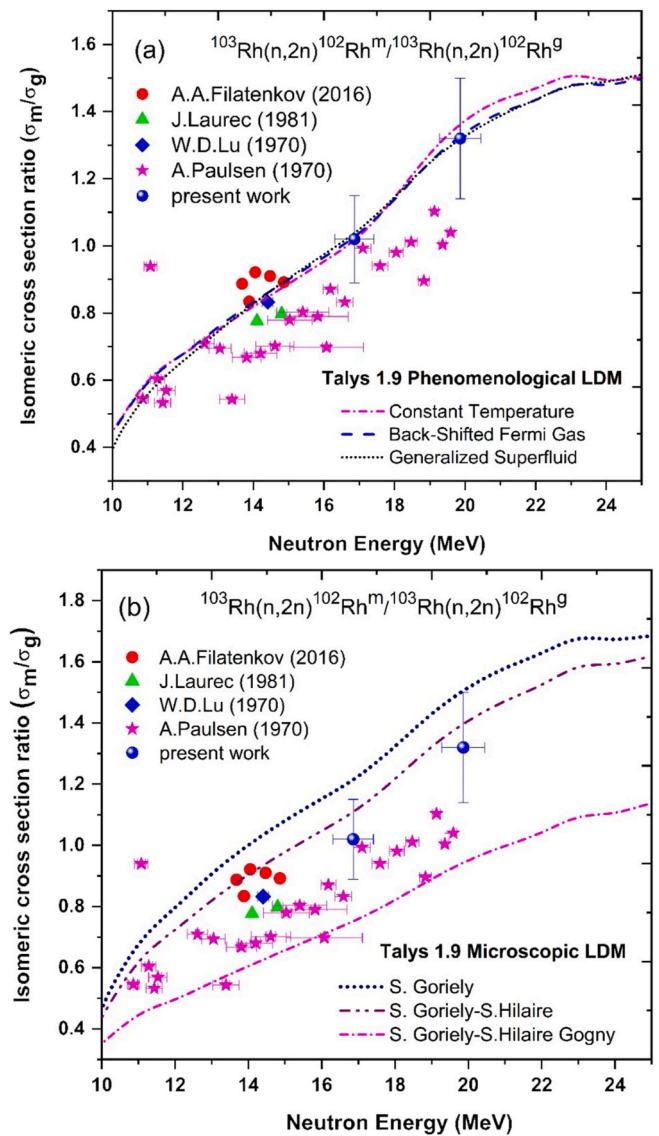

Fig. 9. Measured isomeric cross section ratio (σ_m/σ_g) and TALYS (ver. 1.95) theoretical calculations based on the phenomenological and microscopic level density models.

of poor resolution. There are very few measurements reported with Ge (Li) detector. Therefore, the discrepancies were observed in reported $(n, 2n)$ and (n, p) reactions cross sections. In addition, to explore the discrepancies among the measured (n, p) reaction cross sections of the ^{48}Ti and ^{52}Cr fusion reactor structure materials, the theoretical estimations were conducted using the statistical TALYS code. The various level density models from phenomenological to microscopic were used to calculate theoretical (n, p) reaction cross sections. The contribution of the pre-equilibrium process at higher energies was done by using different pre-equilibrium models. The theoretical results from the TALYS code were compared and discussed with reported previous experimental data of the ^{48}Ti and ^{52}Cr elements.

5.1. The ^{103}Rh $(n, 2n)^{102}$Rh^m and ^{103}Rh $(n, 2n)^{102}$Rh^g reactions

In the present work, the mapping of excitation functions for the ^{103}Rh $(n, 2n)^{102}$Rh^m and ^{103}Rh $(n, 2n)^{102}$Rh^g reactions were performed experimentally at the two different neutron energies and theoretically for the first time from the reaction threshold to 25 MeV. These previous measurements reported in the literature (Fotiades et al., 2016;
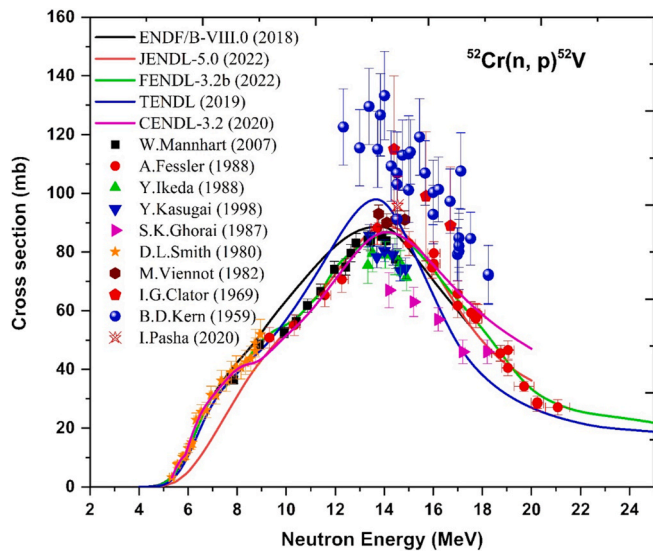
Fig. 10. Literature cross sections compared with the latest evaluated data libraries.

Filatenkov, 2016; Paulsen and Widera, 1970; Laurec and Adam, 1981; Lu Ranakumar et al., 1970; Bormann Bissem et al., 1970) and present experimental results were used to validate the theoretical estimations of the TALYS (ver. 1.95) code by considering the various level density, preequilibrium, and optical potential models available in the code. The results for the isomeric and ground state cross section based on the phenomenological and microscopic level density models and default Koning-Delaroche optical potential, numerical transition rates with energy-dependent matrix element (preeqmode 2) preequilibrium and γ-ray strength functions Kopecky-Uhl models are presented in Fig. 5 (a–b) and 6(a–b).

As can be seen, the previous measurements of the isomeric state cross section are only limited to a narrow energy range of 13.5–15.0 MeV (Filatenkov, 2016; Laurec and Adam, 1981), whereas data of the Fotiades et al. (2016), Paulsen and Widera (1970) and Lu Ranakumar et al. (1970) demonstrates significant discrepancies. The theoretical results for the isomeric state cross section based on the phenomenological and microscopic level density models are presented in Fig. 5(a) and (b). The results show that the back-shifted Fermi gas model describes quite well the cross section data of Filatenkov (2016) and Laurec and Adam (1981) and it also follows the trend of the present experimental results at 19.89 MeV within experimental uncertainties. However, the generalized superfluid model does not reproduce the experimental data of the present work as well as the previous literature data within 13–18 MeV, whereas the constant temperature model follows the trend of the present experimental results at 16.86 MeV and higher energies data of Laurec and Adam (1981). The microscopic calculations by S. Goriely and S. Goriely-S. Hilaire overestimated the cross section compared to the reported data of Filatenkov (2016) and Laurec and Adam (1981) and S. Goriely-S. Hilaire performs very well for the experimental data of the present work at 16.86 MeV. The theoretical trend of the S. Goriely-S. Hilaire Gogny model is less satisfactory compared to the other two microscopic models with the experimental data.

As can be seen, the previous measurements of the ground state cross section also demonstrated significant discrepancies. As shown in Fig. 6 (a), the ground state results of the back-shifted Fermi gas and generalized superfluid models perform excellently for the present data at 19.89 MeV and the latest data reported by Filatenkov (2016) and Bormann Bissem et al. (1970). The theoretical predictions based on the constant temperature models agree with the data of Fotiades et al. (2016) and Laurec and Adam (1981) from the 13–14 MeV region and present

experimental results at 16.86 MeV. These theoretical calculations are consistent with most of the literature data and present experimental work. Similarly, the microscopic calculations for the ground state based on the S. Goriely-S. Hilaire and S. Goriely-S. Hilaire Gogny shows good agreement with the reported data of Fotiades et al. (2016), Filatenkov (2016), and Bormann Bissem et al. (1970) and present study at 19.89 MeV as shown in Fig. 6(b). However, the microscopic calculations for the ground state based on the S. Goriely shows good agreement with the reported data of the present study at 16.86 MeV.

5.2. The ^{103}Rh $(n, 2n)^{102}Rh$ reaction

The present experimental results of the ^{103}Rh $(n, 2n)^{102}Rh$ reaction are shown in Fig. 7 and values are presented in Table 4 along with their uncertainties. The measured cross sections are compared with literature data (Filatenkov, 2016; Paulsen and Widera, 1970; Frehaut et al., 1980; Veeser et al., 1977; Mather et al., 1972; Vallis, 1966; Tewes et al., 1960), evaluated data libraries (Brown Chadwick et al., 2018; Ge et al., 2020; Koning Rochman et al., 2019; Iwamoto Shibata et al., 2022; Forrest et al., 2022) and with the theoretical calculations. As can be seen, the measured experimental data of Filatenkov (2016), Frehaut et al. (1980) and Veeser et al. (1977) show good agreement with the evaluated data of the ENDF/B-VIII.0 and JENDL-5.0 libraries within experimental uncertainties. Our results at the average neutron energy of 16.86 MeV are higher than the evaluation by the TENDL-2019 data library and show good agreement with the evaluated data of the JENDL-5.0, ENDF/B-VIII.0 and FENDL-3.2b libraries. A good agreement is found between the experimental data of the present work and those of Veeser et al. (1977) at 16.86 MeV, whereas present results at 19.89 MeV follow the trend of the TENDL-2019 and FENDL-3.2b data library within experimental uncertainties. In contrast, the reported measured data of Paulsen and Widera (1970), Vallis (1966) and Tewes et al. (1960) show lower values of cross section compared to the latest evaluated data.

The theoretical results based on the phenomenological and microscopic level density models are shown in Fig. 8(a–d). The theoretical calculations using TALYS code based on the default Koning-Delaroche optical potential models, numerical transition rates with energy-dependent matrix element (preeqmode 2) preequilibrium and γ-ray strength functions Kopecky-Uhl using different level densities models are shown in Fig. 8(a–c). In the case of level density models, almost all recent experimental data are in the range of theoretical calculations, except the data reported by Paulsen and Widera (1970), Vallis (1966) and Tewes et al. (1960) above 10 MeV energies. As shown in Fig. 8(a), the present measurements at 16.86 and 19.89 MeV are in good agreement with the theoretical calculation based on the constant temperature level density model. The generalized superfluid model fails to reproduce the cross section of Filatenkov (2016) and Veeser et al. (1977). At the near threshold of 13 MeV energies, theoretical prediction based on the constant temperature model diverges from the experimental data. The back-shifted Fermi gas model calculation is in good agreement with the data of Filatenkov (2016) and the present measurement at 19.89 MeV [see Fig. 8(a)]. Similarly, the theoretical results of S. Goriely and S. Goriely-S. Hilaire calculation agreed with our results at 16.86 MeV and data of Filatenkov (2016), L. R. Veeser et al. (1977) and Mather et al. (1972), whereas all three microscopic level density models are following the trend of experimental data of Veeser et al. (1977) above 18 MeV [see Fig. 8(b)].

Furthermore, the EMPIRE code was also used for theoretical calculations using several models of level density and default Koning-Delaroche optical potential model, Modified Lorentzian (MLO1) γ-ray strength functions, preequilibrium exciton model (PCROSS = 1.5 default) models, the optimal combination of the models is given in Table 5. Note that among the three phenomenological level density models, the EMPIRE calculations based on the Empire-specific level density model show good agreement with the reported data of Filatenkov (2016), Frehaut et al. (1980) and Veeser et al. (1977) as well as
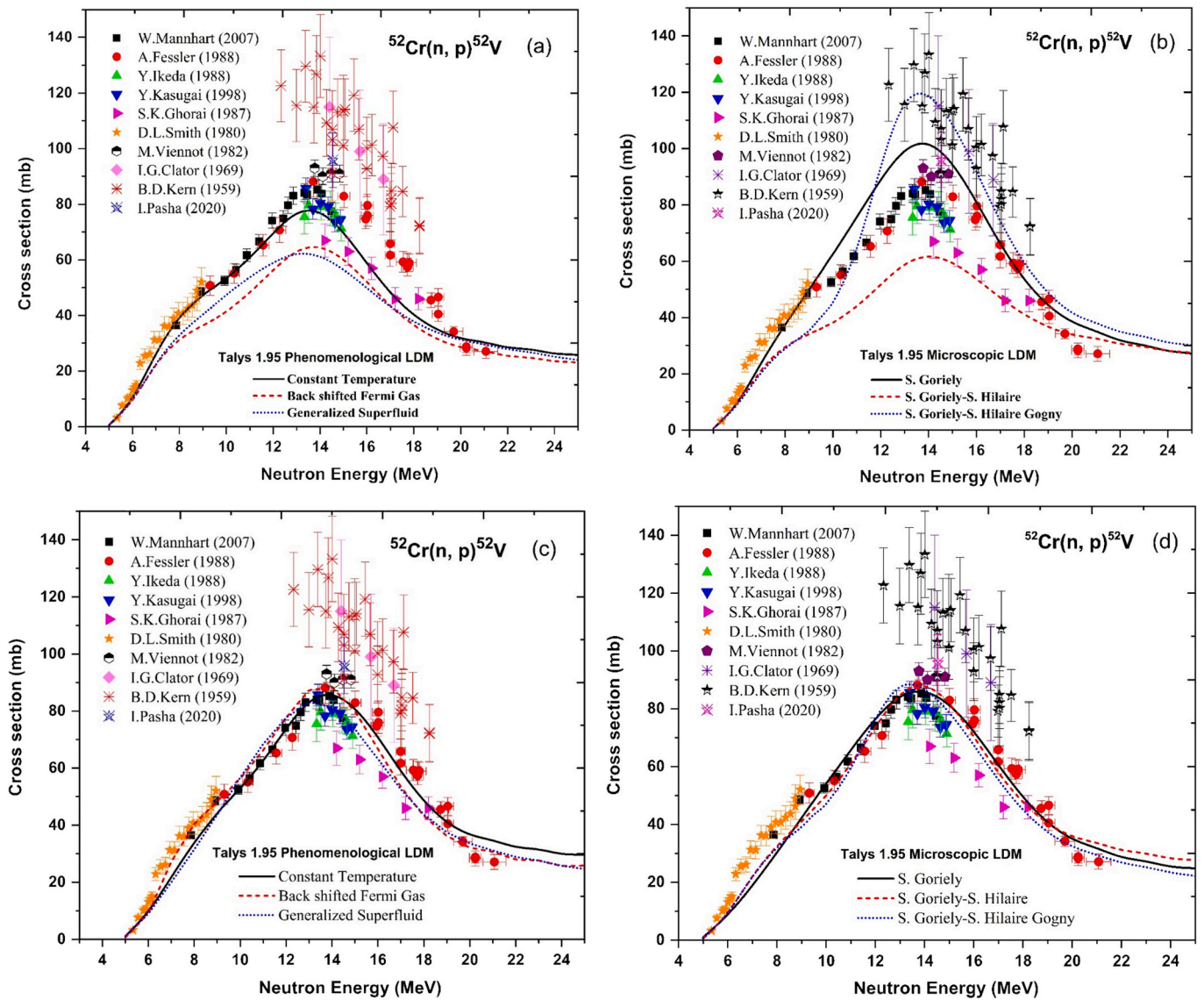

Table 6
Theoretical models and optimum parameters are used in TALYS calculations to reproduce the data of ^{48}Ti and ^{52}Cr isotopes.

Nuclide	level density models	preequilibrium model	optical potential model	level density parameters	Keywords
^{48}Ti	Constant temperature	preeqmode 2	dispersion y	alphald 0.07996	fullhf
				betald 0.27276	asys
	Back-shifted Fermi gas	preeqmode 2	jlmomp y	alphald 0.07796	fullhf
				betald 0.18276	gshell
				gammald 0.051	
	Generalized superfluid	preeqmode 2	dispersion y	alphald 0.1336	fullhf
				betald 0.03092	
	S. Goriely	preeqmode 3	jlmomp y	ctable −0.0921	fullhf
				ptable 0.2741	
	S. Goriely-S. Hilaire	preeqmode 3	jlmomp y	ctable −0.0921	fullhf
				ptable 0.2741	
	S. Goriely-S. Hilaire Gogny force	preeqmode 2	jlmomp y	ctable −0.0921	fullhf
				ptable 0.2741	
^{52}Cr	Constant temperature	preeqmode 1	jlmomp y	alphald 0.06326	fullhf
				betald 0.2728	
				widthmode 0	
				strength 1	
	Back-shifted Fermi gas	preeqmode 1	dispersion y	alphald 0.06426	fullhf
				betald 0.19531	
				gammald 0.051	
	Generalized superfluid	preeqmode 2	jlmomp y	alphald 0.1226	fullhf
				betald 0.03536	asys
	S. Goriely	preeqmode 1	jlmomp y	ctable −0.1005	fullhf
				ptable −0.20419	gshell
				a 11.22	
				strength 1	
				widthmode 2	
	S. Goriely-S. Hilaire	preeqmode 2	localomp	ctable 0.1650	fullhf
				ptable −0.20419	
				deltaW −0.61442	
				pairconstant 10.3	
	S. Goriely-S. Hilaire Gogny force	preeqmode 2	localomp n	ctable 0.1005	fullhf
				ptable −0.20419	gshell
				preeqspin 3	
				deltaW 0.6142	
				pair 3.124	
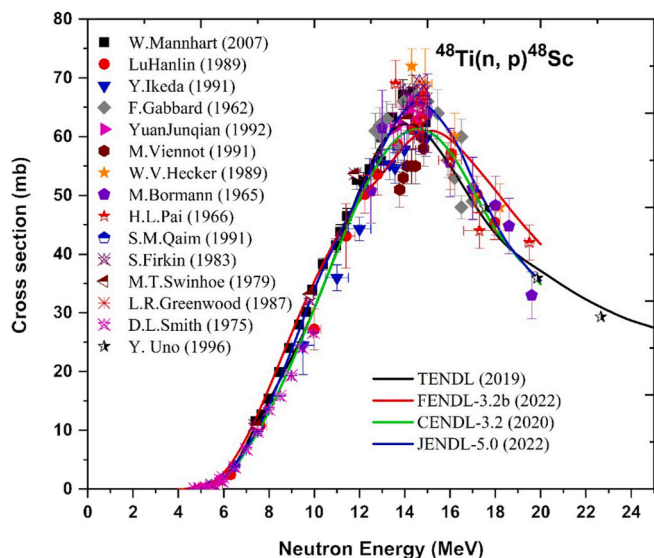
Fig. 12. Literature cross sections compared with the latest evaluated data libraries.

Meadows (1980) reported the measured cross sections. In this region, there are no contributions from the ^{53}Cr $(n, np)^{52}$V and ^{53}Cr $(n, d)^{52}$V reactions since the reaction threshold energies are 11.34 and 9.07 MeV, respectively. Hence measurements carried out using a natural sample of chromium give a pure ^{52}Cr $(n,p)^{52}$V reaction cross section. As shown in Fig. 10, the measured cross sections of Mannhart and Schmidt (2007),

Fessler et al. (1998) and Smith and Meadows (1980) agree very well with the FENDL-3.2b and CENDL-3.2 evaluation and are in fair agreement with TENDL-2019, ENDF-B/VIII.0 and JENDL-5.0 libraries. It is worth mentioning that at around 14–15 MeV neutron energy where multiple measured data are available, the data agree with each other within 10%, whereas the data from Ghorai et al. (1987), Clator (1969) and Kern et al. (1959) are either too high or too low and there is no consistent agreement among them. Above 14 MeV incident neutron energy, all the measured cross sections show different values above or below the evaluated cross section data. The measured data by Ghorai et al. (1987) around 14 MeV deviate too much from all existing measured cross sections, and the true excitation curve does not seem to follow the trend of this data set, because measured data below 12 MeV neutron energy are quite accurate and the contribution from the ^{53}Cr $(n, x)^{52}$V reaction is zero or negligibly small.

The obtained theoretical results from the TALYS code based on the phenomenological and microscopic level density models and default Koning-Delaroche optical potential, numerical transition rates with energy-dependent matrix element (preeqmode 2) preequilibrium and γ-ray strength functions Kopecky-Uhl models are presented in Fig. 11 (a–d). For all these calculations, various phenomenological and microscopic level density models were parameterized as given in Table 5. The theoretical cross section of ^{52}Cr $(n, p)^{52}$V reaction was compared with previous results of Pasha et al. (2020), Mannhart and Schmidt (2007), Fessler et al. (1998), Kasugai Yamamoto et al. (1998), Ikeda et al. (1988), Ghorai et al. (1987), Viennot and Paic (1982), Smith and Meadows (1980), Clator (1969) and Kern et al. (1959). The theoretical trends presented in Fig. 11(a), are based on the phenomenological model of the level densities. The calculation, which uses the optical model of Koning and Delaroche and the modified Lorentzian model for the γ-ray strength functions, reproduces the previous results at lower
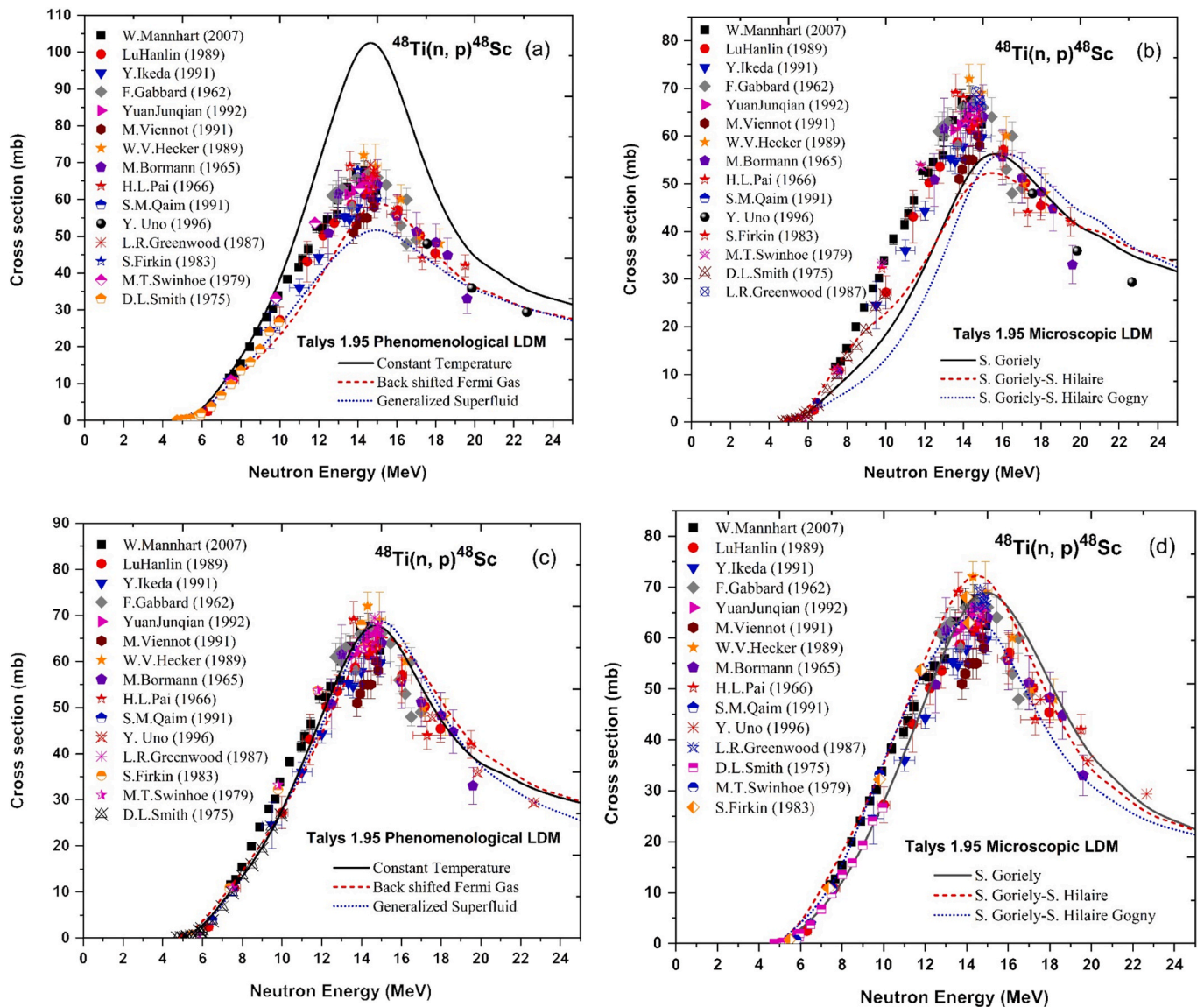
Fig. 13. Literature cross sections compared with the TALYS (ver. 1.95) calculations based on the phenomenological and microscopic level density models (a–b) Default and (cd) Adjusted.

energies and the high energy part of the excitation function. A comparison with the model calculation shows that in the energy range of 11–20 MeV, the constant temperature model systematically underestimates the experimental data. The Koning and Delaroche optical potential and the Kopecky and Uhl γ-strength functions allow better data reproduction at the near-threshold energies. Above 15 MeV, the data by Ghorai et al. (1987) agree with the calculated values from the TALYS code. However, the reported data by Kern et al. (1959) within the neutron energies of 12–20 MeV are systematically higher than the data of literature and theoretical values from the TALYS code. In Fig. 11(b), the theoretical calculations resulting from the TALYS code are presented, but this time using three microscopic models for the level density calculations. Among these, the model described by Goriely et al. (microscopic model 2) exhibits the best behaviour since it accurately describes the energy areas examined in the earlier measurements. The data reproduction of the Goriely et al. (microscopic model 1) microscopic model is also quite good. The behaviour of the microscopic model was improved by combining it with the semi-microscopic optical potential of the Bauge et al. exciton pre-equilibrium model and a microscopic model for the strength functions based on Hartree-Fock-Bogolyubov calculations as shown in Fig. 11(d). The

resulting fit for the ^{52}Cr $(n,p)^{52}$V reaction cross section is illustrated in Fig. 11(c–d). The level density parameters and the adjustments adapted to fit the experimental data using the TALYS code are given in Table 6. The theoretical excitation function of the (n,p) reaction for ^{52}Cr using adjustments is in substantially better agreement with the literature data compared to the calculations with default parameters.

5.5. The ^{48}Ti $(n,p)^{48}$Sc reaction

The excitation function of the ^{48}Ti $(n,p)^{48}$Sc reaction along with the reported measured (Mannhart and Schmidt, 2007; Uno Meigo et al., 1996; Lu et al., 1989; Yuan et al., 1992; Ikeda Konno et al., 1991; Qaim et al., 1991; Viennot Berrada et al., 1991; Hecker et al., 1989; Greenwood, 1987; Firkin, 1983; Swinhoe and Uttley, 1979; Smith and Meadows, 1975; Pai, 1966; Bormann et al., 1965; Gabbard and Kern, 1962) and evaluated data libraries (Brown Chadwick et al., 2018; Ge et al., 2020; Koning Rochman et al., 2019; Iwamoto Shibata et al., 2022; Forrest et al., 2022) is shown in Fig. 12. A good agreement among literature data has been found within experimental uncertainties except with the few data, probably due to the use of old nuclear decay data and monitor values in those analyses. These reported cross sections were

measured by many labs and there is a large discrepancy in the energy region of 13–16 MeV. Below 13 MeV, the ^{48}Ti $(n,p)^{48}$Sc reaction was studied in various previous measurements (Mannhart and Schmidt, 2007; Uno Meigo et al., 1996; Lu et al., 1989; Yuan et al., 1992; Ikeda Konno et al., 1991; Qaim et al., 1991; Viennot Berrada et al., 1991; Hecker et al., 1989b; Greenwood, 1987; Firkin, 1983; Swinhoe and Uttley, 1979; Smith and Meadows, 1975; Pai, 1966; Bormann et al., 1965; Gabbard and Kern, 1962) and the latest TENDL-2019, FENDL-3.2b, JENDL-5.0 and CENDL-3.2 evaluation reproduces the previous experimental data well. The evaluation follows the measurements up to 13 MeV and is different in values above 13 MeV energies. At energies above 14 MeV, the latest evaluated data JENDL-5.0 is 10% higher than the evaluated data of the CENDL-3.2 library. It's observed that the high energies data of Uno Meigo et al. (1996) follow the trend of evaluated data of the TENDL-2019 library. However, above 15 MeV, the reported data of Lu et al. (1989), Pai (1966), Bormann et al. (1965) and Gabbard and Kern (1962) show agreement with the evaluated data within experimental uncertainties.

The theoretical results based on the phenomenological and microscopic level density models and default Koning-Delaroche optical potential, numerical transition rates with energy-dependent matrix element (preeqmode 2) preequilibrium and γ-ray strength functions Kopecky-Uhl models are presented in Fig. 13(a–d). Initially, for all these default calculations phenomenological and microscopic level density, preequilibrium, and optical potential models were used as mentioned in Table 5. The theoretical estimation of the ^{48}Ti $(n,p)^{48}$Sc reaction was compared with the previous experimental results of Mannhart and Schmidt (2007), Uno Meigo et al. (1996), Lu et al. (1989), Yuan et al. (1992), Ikeda Konno et al. (1991), Qaim et al. (1991), Viennot Berrada et al. (1991), Hecker et al. (1989b), Greenwood (1987), Firkin (1983), Swinhoe and Uttley (1979), Smith and Meadows (1975), Pai (1966), Bormann et al. (1965) and Gabbard and Kern (1962). It is observed that these default theoretical results based on the phenomenological and microscopic models failed to reproduce the literature data from threshold to 25 MeV are shown in Fig. 13(a–b). The theoretical calculations were improved using different models and adjusting the parameters available in the TALYS code to reproduce the experimental data. The theoretical trend of the ^{48}Ti $(n,p)^{48}$Sc cross section from the statistical model calculations after adjusting the parameters is shown in Fig. 13(c–d). However, we have shown that the trend of the experimental data can be reproduced with a statistical model TALYS code with appropriate adjustments made to the microscopic level density parameters 'ctable' and 'ptable' [see Fig. 13(d)]. Similarly, the appropriate adjustments were made to the phenomenological level density parameters alphald, betald and gammald to reproduce the experimental data as shown in Fig. 13(c). The level density parameters and the different theoretical model adjustments adapted to reproduce the previously measured experimental data are given in Table 6.

6. Summary and conclusions

The ^{103}Rh $(n,2n)^{102}$Rh^g and ^{103}Rh $(n,2n)^{102}$Rh^m reactions cross sections were measured at two different energies using quasi-monoenergetic neutrons from the BARC-TIFR Pelletron accelerator facility Center India. Neutron induced $(n,2n)$ reaction cross sections were measured relative to the ^{27}Al $(n,\alpha)^{24}$Na reaction using the method of neutron activation followed by off-line γ-ray spectrometry. It is found that the present experimental results of isomeric and ground state are in good agreement with the literature data and the total cross sections follows the trend of the latest evaluated FENDL-3.2b data. Moreover, the present measurements and the existing cross section data reported in the EXFOR database have been reproduced based on the default theoretical calculations using the TALYS (ver. 1.95) and EMPIRE (ver. 3.2.3) reaction codes. It was concluded that the phenomenological constant temperature level density model has a better behaviour for the ground, isomeric, total and isomeric cross section ratio of the $(n,2n)$ reaction

cross section when is combined with potential of Konning Delaroche, exciton preequilibrium model and Kopecky-Uhl calculations for the γ-ray strength function. However, the theoretical calculations form the EPMPIRE-specific level density model also follows the trend of the present measurements and existing literature data.

Initially, the behaviour of the excitation function was investigated as a function of the different level density models and default pre-equilibrium exciton model, optical potential local Konning-Delaroche and γ-ray strength function Kopecky-Uhl for ^{52}Cr $(n,p)^{52}$V and ^{48}Ti $(n,p)^{48}$Sc reactions provided by the statistical TALYS code and it was concluded that the default calculations failed to reproduce the existing literature data. A better reproduction of the experimental data was successfully achieved when the phenomenological and microscopic level density models were adjusted with the available optical potential, preequilibrium models and level density parameters of level densities models.

Furthermore, it was concluded that when the probability of nuclear reaction is high, the excitation functions generated by pre-equilibrium models in the calculations are heavily influenced by differing level densities. As a result, level densities significantly impact the reaction cross sections. For these nuclear reactions, exciton preequilibrium model predictions are generally precise. These new sets of estimated cross section data, we believe will aid in the understanding of neutron induced $(n,2n)$ and (n,p) processes. Both statistical codes reproduced well the ground, isomer and total cross section with a slightly different set of level densities parameters. In this way, a more systematic investigation of the theoretical calculations can be achieved with new sets of input parameters and theoretical models of level densities, preequilibrium, optical potential and γ-rays strength functions. This work has contributed to understanding $(n,2n)$ and (n,p) reactions on the ^{103}Rh, ^{52}Cr and ^{48}Ti isotopes.

CRediT authorship contribution statement

R.K. Singh: Writing – original draft. **N.L. Singh:** Writing – review & editing. **Mayur Mehta:** Visualization. **Rakesh Chauhan:** Visualization. **S.V. Suryanarayana:** Visualization. **Rajnikant Makwana:** Visualization. **B.K. Nayak:** Visualization. **H. Naik:** Visualization. **Jan Varmuza:** Visualization. **K. Katovsky:** Visualization.

Declaration of competing interest

The authors declare the following financial interests/personal relationships which may be considered as potential competing interests: RatanKumar Singh reports financial support was provided by Inter-University Accelerator Centre.

Data availability

Data will be made available on request.

References

Arrigo, A.D., Giardina, G., Herman, M., Ignatyuk, A., et al., 1994. J. Phys. G 20, 365.
Axel, P., 1962. Phys. Rev. 126, 671.
Bauge, E., Delaroche, J.P., Girod, M., 2001. Phys. Rev. C 63, 024607.
Bormann, M., Bissem, H.H., et al., 1970. Nuclear Physics, Section A 157, 481.
Bormann, M., Fretwurst, E., Schehka, P., et al., 1965. Nucl. Phys. 63, 438.

Brady, F.P., Romero, J.L., 1990. Nucl. Sci. Eng. 106, 318–331.

Brink, D.M., 1957. Nucl. Phys. 4, 215.

Brown, D.A., Chadwick, M.B., et al., 2018. EDNF/B-VIII.0. Nucl. Data Sheets 148, 1–142.

Capote, R., Herman, M., et al., 2009. Ripl – reference input parameter library for calculation of nuclear reactions and nuclear data evaluations. Nucl. Data Sheets 110, 3107–3214.

Capote, R., Zolotarev, K.I., et al., 2014. International Reactor Dosimetry and Fusion File IRDFF v.1.05. IAEA Technical Report No. INDC(NDS)-0616, 9 Oct.

Clator, I.G., 1969. Neutron Induced Reactions between 14.4 and 16.7 MeV Thesis. Clator.

De Frenne, D., 2009. Nucl. Data Sheets 110, 1745.

Dilg, W., Schantl, W., Vonach, H., Uhl, M., 1973. Nucl. Phys. A 217, 269.

Fessler, A., Wattecamps, E., Smith, D.L., 1998. Phys. Rev. Part C, Nucl. Phys. 58, 996.

Filatenkov, A.A., 2016. "Neutron Activation Cross Sections Measured at KRI in Neutron Energy Region 13.4 – 14.9 MeV" IAEA Nuclear Data Section. Vienna International Centre, A-1400 Vienna, Austria.

Firestone, R.B., 2007. Nucl. Data Sheets 108, 2319.

Firkin, S., 1983. A.E.R.E. Harwell Reports, No.3350.

Forrest, R.A., Capote, R., Otsuka, N., et al., 2022. FENDL-3.2b Fusion Evaluation Nuclear Data Library. IAEA. INDC (NDS)-0628.

Fotiades, N., Devlin, M., Nelson, R.O., et al., 2016. Phys. Rev. C 94, 044608.

Frehaut, J., Bertin, A., Bois, R., Jary, J., 1980. U.S. report to the I.N.D.C., No.84, vol. 1, p. 399.

Gabbard, F., Kern, B.D., 1962. Phys. Rev. 128, 1276.

Ge, Zhigang, Xu, Ruirui, Wu, Haicheng, et al., 2020. CENDL-3.2: the new version of Chinese general purpose evaluated nuclear data library. EPJ Web Conf. 239, 09001.

Georgali, E., Eleme, Z., Patronis, N., Aslanoglou, X., et al., 2018. Phys. Rev. C 98, 014622.

Ghorai, S.K., Williams, J.R., Aford, W.L., 1987. J. Phys. G 13, 405.

Gilbert, A., Cameron, A.G.W., 1965. Can. J. Phys. 43, 1446.

Goriely, S., Tondeur, F., Pearson, J.M., 2001. Atomic Data Nucl. Data Tables 77, 311.

Goriely, S., Hilaire, S., Koning, A.J., 2008a. Phys. Rev. C 78, 064307.

Goriely, S., Hilaire, S., Koning, A.J., 2008b. Phys. Rev. C 78, 064307.

Greenwood, L.R., 1987. Am. Soc. Test. Mater. Rep. 956, 743.

Hauser, W., Feshbach, H., 1952. Phys. Rev. 87, 366.

Hecker, W.V., et al., 1989a. Nucl. Instrum. Methods Phys. Res., Sect. B 40–41, 478.

Hecker, W.V., et al., 1989b. Nucl. Instrum. Methods Phys. Res., Sect. B 40–41, 478.

Herman, M., Capote, R., Sin, M., et al., 2007. EMPIRE-3.2.3 statistical model code for nuclear reaction calculations and nuclear data evaluation. Nucl. Data Sheets 108, 2655.

Hilaire, S., Girod, M., Goriely, S., Koning, A.J., 2012. Phys. Rev. C86, 064317.

Hofmann, H.M., Richert, J., Tepel, J.W., et al., 1975. Ann. Phys. (N.Y.) 90, 403.

Ignatyuk, A.V., Istekov, K.K., Smirenkin, G.N., 1979. Sov. J. Nucl. Phys. 29, 450.

Ignatyuk, A.V., Weil, J.L., Raman, S., Kahane, S., 1993. Phys. Rev. C 47, 1504.

Ikeda, Y., Konno, C., Oishi, K., Nakamura, T., et al., 1988. JAERI Reports, No. 1312.

Ikeda, Y., Konno, C., et al., 1991. Conf. on Nucl. Data for Sci.and Technol.,Juelich 1991, p. 294.

Iwamoto, O., Shibata, K., et al., 2022. Japanese Evaluated Nuclear Data Library Version 5: JENDL-5 in preparation.

Jungerman, J.A., Brady, F.P., et al., 1971. Nucl. Instrum. Methods 94, 421–427.

Kalbach, C., 1986. Phys. Rev. C 33, 818.

Kasugai, Y., Yamamoto, H., et al., 1998. Ann. Nucl. Energy 25 (Issue.1–3), 23.

Kern, B.D., Thompson, W.E., Ferguson, J., 1959. Nucl. Phys. 10, 226.

Koning, A.J., Delaroche, J.P., 2003. Nucl. Phys. A 713, 231.

Koning, A.J., Duijvestijn, M.C., 2004. Nucl. Phys. A 744, 15.

Koning, A.J., et al., 2018. TALYS (Ver. 1.95), A Nuclear Reaction Program, User Manual, NRG-1755 ZG Petten, The Netherlands.

Koning, A.J., Rochman, D., et al., 2019. TENDL-2019. Nucl. Data Sheets 155, 1–55.

Kopecky, J., Uhl, M., 1990. Phys. Rev. C 41, 1941.

Laurec, J., Adam, A., 1981. T. De Bruyne Centre 'Etudes Nucleaires, Saclay Reports, No. 5109.

Lu, Hanlin, Zhao, Wenrong, et al., 1989. Chinese Report to the I.N.D.C., No.16.

Lu, W.D., Ranakumar, N., et al., 1970. Phys. Rev., Part C, Nucl. Phys. 1, 350.

Mannhart, W., Schmidt, D., 2007. Phys. Techn. Bundesanst., Neutronenphysik Reports, No. 53.

Mather, D.S., Bampton, P.F., Coles, R.E., James, G., Nind, N.J., 1972. "Measurement of (n, $2n$) Cross Sections for Incident Energies between 6 and 14 MeV" United Kingdom. N. P.

McNaughton, M.W., King, N.S.P., et al., 1975. Nucl. Instrum. Methods 130, 555–557.

Midhun, C.V., Musthafa, M.M., et al., 2021. Phys. Rev. C 104, 054606.

Nishioka, H., Verbaarschot, J.J.M., Weidenmuller, H.A., et al., 1986. Ann. Phys. 172, 67.

Otuka, N., Dupont, E., et al., 2014. Nucl. Data Sheets 120, 272–276.

Otuka, N., Lalremruata, B., Khandake, M.U., et al., 2017. Radiat. Phys. Chem. vol. 140, 502–510.

Pai, H.L., 1966. Can. J. Phys. 44, 2337.

Pasha, I., Rudraswamy, B., Santhi, S.Y., et al., 2020. Radiochim. Acta 108, 679.

Paulsen, A., Widera, R., 1970. Z. Phys. 238, 23–34.

Plujko, V.A., 2000. Acta Phys. Pol. B 31, 435.

Qaim, S.M., et al., 1991. Conf. on Nucl. Data for Sci. and Technol., Juelich 1991, p. 297.

Singh, R.K., Singh, N.L., Chauhan, R.D., et al., 2021. Eur. Phys. J. A 57, 337.

Singh, R.K., Singh, N.L., Chauhan, R.D., et al., 2022. Chin. Phys. C 46 (5), 054002.

Smith, D.L., Meadows, J.W., 1975. Nucl. Sci. Eng. 58, 314.

Smith, D.L., Meadows, J.W., 1980. Nucl. Sci. Eng. 76, 43.

Smith, D.L., et al.. Corrections for Low Energy Neutrons by Spectral Indexing. NEA/ WPEC-XX, Volume XX. https://www.oecd-nea.org/upload/docs/application/pd f/2020-01/nsc-wpec-doc2005-357.pdf. pg. No. 143.

Swedish Nuclear Fuel and Waste Management Co, ISSN 1402–3091, 2008. SKB Rapport on Fusion Driven Systems (FDS) for Transmutation, R-08-126.

Swinhoe, M.T., Uttley, C.A., 1979. A.E.R.E. Harwell Reports, No. 26, p. 39.

Tamura, T., Udagawa, T., Lenske, H., 1982. Phys. Rev. C 26, 379.

Tewes, H.A., Caretto, A.A., Miller, A.E., Nethaway, D.R., 1960. Excitation Functions of Neutron-Induced Reactions U.C. Lawrence Rad.Lab. (Berkeley and Livermore). No.6028-T.

Uno, Y., Meigo, S., et al., 1996. Internat. Symposium on Reactor Dosimetry, Prague, 1996, p. 465.

Uwamino, Yoshitomo, Soewarsono, Titik Suharti, et al., 1997. Nucl. Instrum. Methods Phys. Res. 389, 463–473.

Vallis, D.G., 1966. Cross sections for (n, $2n$) reaction at 14.7 MeV of some odd-proton nuclei. In: A.W.R.E. Aldermaston Reports, No.76/66.

Veeser, L.R., Arthur, E.D., Young, P.G., 1977. Phys. Rev. C 16 (5).

Viennot, M., Paic, G., 1982. Conf. on Nucl. Data for Sci. and Technol., Antwerp. 1982, p. 406.

Viennot, M., Berrada, M., et al., 1991. Nucl. Sci. Eng. 108, 289.

Yuan, Junqian, Wang, Yongchang, et al., 1992. High Energy Physics and Nucl.Phys., Chin.ed. 16 (1), 57.